PAPER

Exploring correlation effects and volume collapse during electride dimensionality change in Ca$_2$N†

Dmitry Y. Novoselov, (iD) *[abc] Mary A. Mazannikova, (iD) [abc] Dmitry M. Korotin, (iD) [ab]
Alexey O. Shorikov, (iD) [abc] Vladimir I. Anisimov[abc] and Artem R. Oganov (iD) [b]

We investigate the role of interstitial electronic states in the metal-to-semiconductor transition and the origin of the volume collapse in Ca$_2$N during the pressure-induced phase transitions accompanied by changes of electride subspace dimensionality. Our findings highlight the importance of correlation effects in the electride subsystem as an essential component of the complex phase transformation mechanism. By employing a simplified model that incorporates the distortion of the local environment surrounding the interstitial quasi-atom (ISQ) which emerges under pressure and solving this model by Dynamical Mean Field Theory (DMFT), we successfully reproduced the evolution between the metallic and semiconducting phases and captured the remarkable volume collapse. Central to this observation is a significant enhancement of the localization of excess electrons and the emergence of antiferromagnetic pairing among them, leading to a spin-state transition with a notable reduction in the magnetic moment on the interstitial states.

1 Introduction

Recently, there has been a surge of interest in electrides, compounds with unique physical properties whose electrons are confined within crystalline voids.[1–14] The existence of interstitial electrons can significantly affect the physical and chemical characteristics of these materials. It is worth noting that the wave functions describing interstitial electronic states can exhibit both a localized and delocalized character[14,15] and transition between these states can occur due to the change in the dimensionality of the electride subsystem. Since electride energy bands are located in the vicinity of the Fermi level, a change in degree of localization of interstitial electrons can lead to dramatic changes in the observed properties, including transport, thermal, structural, and magnetic ones.

Previous studies[16,17] of the first two-dimensional inorganic layered electride Ca$_2$N have revealed that this system undergoes a series of phase transitions under pressure, accompanied by a consistent reduction in the dimensionality of the region where excess electrons are localized. The anomalous metal-to-

semiconductor transition in Ca$_2$N under pressure, characterized by a sharp increase in resistivity and simultaneous volume collapse, is attributed to this unique characteristic of its electronic subsystem. Similar behavior was observed in elemental lithium, sodium, and calcium.[18–21] The physics of this phenomenon involves a significant increase of the localization degree of electrons in interstitial voids under pressure due to the strong repulsion between valence and inner electrons, arising from orbital overlap. The corresponding wave functions, which satisfy the orthogonality requirement, will be centered on interstitial positions. As a result, the electron density flows from the space around the atoms towards the vacant interstitial positions within the crystal structure. These electrons become quasi-anions and their partially occupied states are situated near the Fermi level. Such states are characterized by significant electron–electron repulsion, leading to substantial correlation effects.[5–8,14] If significant overlap of electride states is possible due to the crystal structure, then splitting into bonding and anti-bonding levels occurs. We propose that this exotic behavior, accompanied by the transition from a 3D to a 0D electride phase, is the primary driving mechanism of energy gap formation and volume collapse in Ca$_2$N under pressure.

2 Results and discussion

2.1 Crystal and band structures

Under normal conditions, Ca$_2$N is a two-dimensional electride with a chemical formula [Ca$_2$N]$^+$·e$^-$. Electrons confined in the

[a] M.N. Mikheev Institute of Metal Physics of Ural Branch of Russian Academy of
Sciences, 18 S. Kovalevskaya St., Yekaterinburg, 620108, Russia.
E-mail: novoselov@imp.uran.ru
[b] Skolkovo Institute of Science and Technology, Bolshoy Blvd., 30, p.1, Moscow
121205, Russia
[c] Department of Theoretical Physics and Applied Mathematics, Ural Federal
University, 19 Mira St., Yekaterinburg, 620002, Russia
† Electronic supplementary information (ESI) available. See DOI: **https://doi.org/
10.1039/d3cp04472f**

voids located between the calcium layers occupy a quasi-anionic site.[7] Dicalcium nitride undergoes a structural transition from the initial layered $R\bar{3}m$ structure to the 3D (previously described as 1D[16]) electride phase with $Fd\bar{3}m$ symmetry[16] under pressure (≈ 2.8 GPa). Fig. 1 shows the isosurfaces of the electron localization function (ELF) for a fragment of the $Fd\bar{3}m$ crystal structure for two ELF values: ELF = 0.75 (a) and ELF = 0.79 (b). In this phase, the interstitial charge density forms a connected charge network with regions of the highest localization near tetrahedral voids between calcium atoms (Wyckoff position 8a). The localization of the electronic density in the center of the calcium tetrahedron is clearly seen in Fig. 1(a) where the isosurface for ELF = 0.75 is drawn.

One can see from the band structure, presented in Fig. 2, that the interstitial electronic states lie in the vicinity of the Fermi level predominantly within the −1.5 to 0.5 eV energy window. The band structure below the electride states is composed of nitrogen p-states and shows some hybridization with the interstitial bands, particularly noticeable at the Γ-point. Note also that the electride states that form the top of the conduction band have a threefold degeneracy at the Γ point protected by crystal symmetry.

Further compression causes a structural transition from the $Fd\bar{3}m$ phase to the 0D electride phase with $I\bar{4}2d$ symmetry,
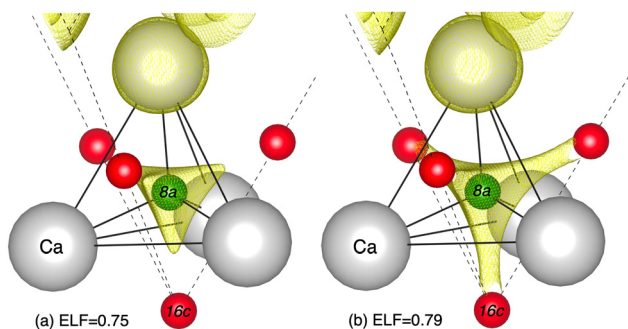
Fig. 1 Isosurface of electron localization function (ELF) for the primitive $Fd\bar{3}m$ cell fragment in the cases of ELF = 0.75 (a) and ELF = 0.79 (b). White spheres correspond to calcium atoms, red and green spheres denote 16c and 8a interstitial Wyckoff positions, nitrogen atoms are hidden for convenience.
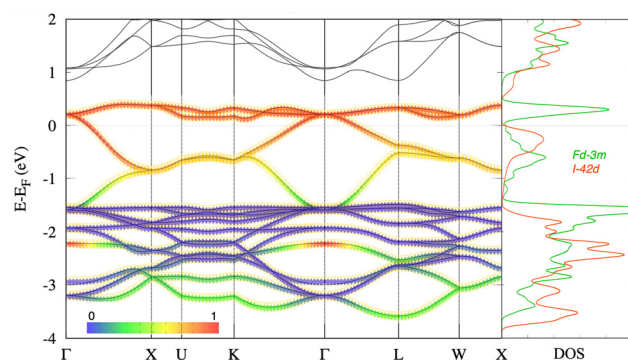
Fig. 2 Band structure of $Fd\bar{3}m$ phase (solid gray curves) and MLWFs with colored projected components of interstitial MLWFs; density of states for $Fd\bar{3}m$ and $I\bar{4}2d$ structures.
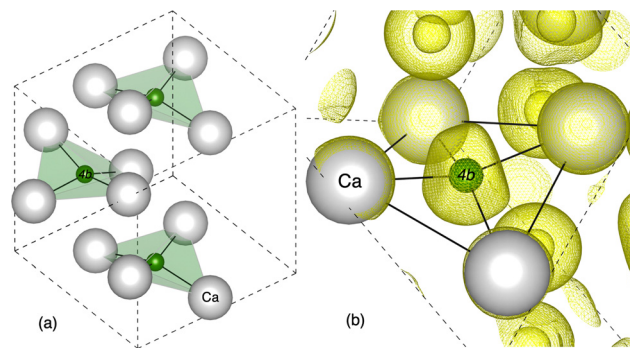
Fig. 3 Schematic view of $I\bar{4}2d$ unit cell (a) and isosurface of ELF = 0.8 (b) for a fragment of $I\bar{4}2d$ structure. White spheres correspond calcium atoms, green spheres denote 4b interstitial Wyckoff positions, nitrogen atoms are hidden for convenience.

which remains stable above 20.5 GPa.[16] This transition occurs with a sharp change in cell volume ($\approx 7\%$) accompanied by the change in electrical resistance corresponding to the transition from metallic to semiconducting behavior.[16] The structural parameters and energy band dispersion of the $I\bar{4}2d$ phase can be found in the ESI.† The analysis of the ELF isosurface for $I\bar{4}2d$ phase (Fig. 3(b)) allows one to identify the region of localization of interstitial charge density at the centers of symmetric but highly compressed tetrahedra (Fig. 3(a)) formed by four calcium atoms in the first coordination sphere of the non-nuclear attractor (Wyckoff position 4b). Thus, the application of external pressure leads to a distortion of the calcium tetrahedron, resulting in a reduction of symmetry of the local environment of the interstitial quasi-atom, lifting the degeneracy of the interstitial electronic states.

Fig. 2 also shows the plots of the density of states for the $Fd\bar{3}m$ and $I\bar{4}2d$ phases. It can be seen from their comparison that during this structural transition the interstitial energy band near the Fermi level becomes spilled into two subbands completely filled and empty, separated by an energy gap.

2.2 Maximally localized Wannier functions

To describe the electronic states of the electride, we constructed Maximally Localized Wannier Functions (MLWFs) projected within the energy window spanned by energy bands in the vicinity of the Fermi level. The Wannier functions of excess anionic electrons in the one-dimensional electride phase of Ca_2N were centered at the 16c Wyckoff positions of the $Fd\bar{3}m$ space group. The isosurface of the four resulting squared electride MLWFs is shown in the left part of Fig. 4. The combination of these four MLWFs forms a molecular orbital centered at the 8a Wyckoff position that is located in the center of the tetrahedral cage formed by the nearest calcium cations (right part of Fig. 4). Both the spatial distribution of this molecular orbital (Fig. 4(b)) and the ELF = 0.75 isosurface (Fig. 1(a)) resemble an orbital with sp³ symmetry. Interstitial electronic states that compose a molecular orbital with sp³-like symmetry represent four-fold degenerate partially filled states.

Since the electride states are hybridized with the p-states of nitrogen atoms, in addition to the interstitial electronic states,

This journal is © the Owner Societies 2023

Phys. Chem. Chem. Phys., 2023, **25**, 30960–30965 | **30961**
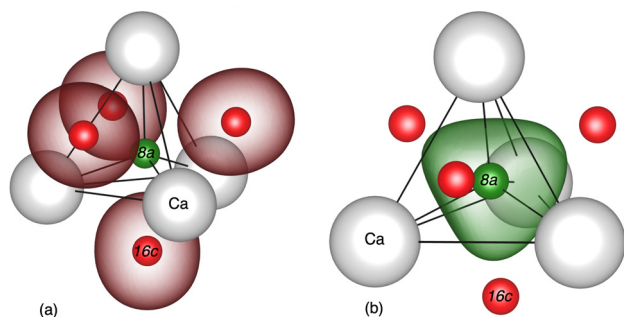
Fig. 4 Isosurface of square of 4 interstitial MLWFs (a) and its sum (b) for $Fd\bar{3}m$ phase. White spheres correspond calcium atoms, red and green spheres denote 16c and 8a interstitial Wyckoff positions, nitrogen atoms are hidden for convenience.

the p-N states were also included in the basis to construct a small non-interacting Hamiltonian. Then the Hamiltonian was diagonalized, corresponding to the transition into the local basis of molecular orbitals, which form the one-dimensional charge network of the electride.

2.3 Hypothesis

Transformation into the local basis set of molecular orbitals leads to the decomposition of the electride electronic subspace into one fully filled and three partially filled orbitals, which exhibit a triple degeneracy similar to the decomposition of sp^3 into one s and three p orbitals (Fig. 5). With the start of the pressure-induced structural phase transition from $Fd\bar{3}m$ to $I\bar{4}2d$, Ca_4 tetrahedra around the "electride" maximum become distorted and this leads to a reduction in the symmetry of the local crystal field of the interstitial quasi-atom. This results in the lifting of the degeneracy of the triply degenerate sub-shell.

Since the interstitial electronic states in the $Fd\bar{3}m$ phase are partially filled and well-localised, significant correlation effects within the Ca_2N electride subsystem are expected, as proposed in paper.[7] These correlations might be responsible for the metal-semiconductor transition and volume collapse.

To verify this hypothesis and to qualitatively reproduce the metal-semiconductor transition with volume collapse, we introduce an additional potential for electride states, simulating the presence of a crystal field distortion. This potential is specifically designed to reproduce an energy split in the Hamiltonian, which lifts the degeneracy of the triply degenerate band. This is accomplished by shifting one level below the sub-shell's center of mass by δ and raising two doubly degenerate levels by $\delta/2$, while maintaining the band center's position (see Fig. 5).
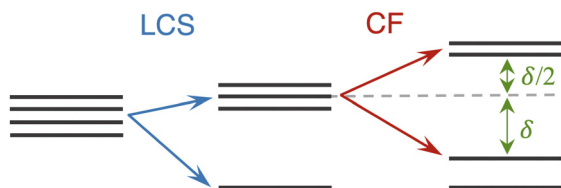
Fig. 5 Sketch of the electride levels splitting in a local coordinate system (LCS) and the model splitting by a distorted crystal field (CF).

2.4 DMFT

The constructed Hamiltonian was solved using the combination of density functional theory (DFT) and dynamical mean field theory, the so-called DFT+DMFT method,[22] which allows one to take into account electronic correlations and many-body effects in the electride subsystem. Calculations were carried out for a set of δ values at a fixed Coulomb parameter U = 2.5 eV, which was previously estimated for Ca_2N.[7] One can see from the density of states presented in Fig. 6, that there are two sets of solutions corresponding to the metallic state with $0.0 \leq \delta \leq 0.2$ (curves in green shades) and the state with an energy gap for $0.3 \leq \delta \leq 0.5$ (curves in yellow-red shades). Therefore, we obtain a clear picture of the metal-to-semiconductor transition occurring at the critical value of the crystal field splitting parameter δ = 0.3 eV.

After applying the external potential, the density of states at the Fermi level first increases and then abruptly drops, and the energy gap opens at δ = 0.3 eV. This behavior occurs since the lower band gradually shifts down with increasing strength of the crystal field, and after reaching the critical value, it splits further due to the Coulomb interaction between the electride electrons. Further enhancement of the crystal field leads to an increase in the energy gap, which is consistent with experimental observations[16] showing a resistivity jump followed by its subsequent increase.

Fig. 7 shows the orbital-resolved density of states for the several solutions: without CF (a), just before and after the transition (b and c), and without electron–electron Coulomb interactions (d). One can see from Fig. 7(a), that in the absence of a distorting crystal field, three states remain degenerate and an energy gap is absent. It is worth noting that, in addition to opening the energy gap during the metal-to-semiconductor transition (Fig. 7(b) and (c)), they exhibit a qualitative difference: In the first case, molecular orbitals 2, 3, and 4 are partially filled, while in the second case, orbital 2 is completely filled, and orbitals 3 and 4, while remaining degenerate, become the conduction band which is typical for the Mott metal-insulator transition. In the absence of Coulomb interaction between interstitial electrons, the presence of a crystal field is insufficient to open an energy gap and create fully occupied and fully empty states (Fig. 7(d)).
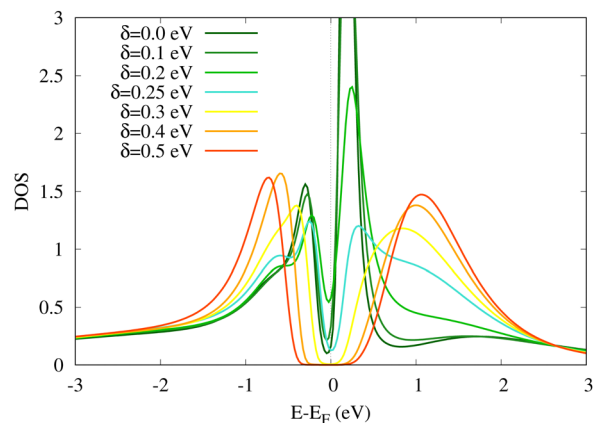
Fig. 6 Dependence of the density of states on energy relative to the Fermi level for different values of δ.

30962 | *Phys. Chem. Chem. Phys.*, 2023, **25**, 30960–30965

This journal is © the Owner Societies 2023
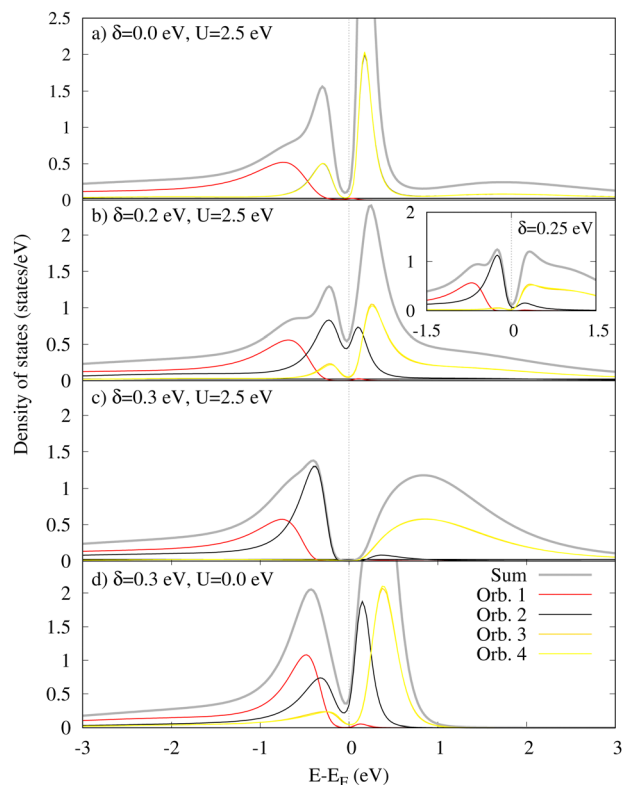
Fig. 7 Orbital-resolved density of states relative to the Fermi level for the cases without distorting CF (a), with $\delta = 0.2$ and $\delta = 0.25$ in the inset (b) and 0.3 eV (c), as well as with $\delta = 0.3$ but with Coulomb parameter $U = 0$ eV (d).

To evaluate pressure, we fit to our total energies the third-order Birch–Murnaghan equation of state[23] for the case without crystal field splitting and for the solution with $\delta = 0.5$ eV at which the magnitude of the energy gap is closest to the value of the gap in the $I\bar{4}2d$ phase.[16,17] Then the enthalpy ($H = E + PV$) for these two solutions was calculated to determine the transition pressure and the change in volume. The resulting phase diagram is shown in Fig. 8. From this figure one can see that the phase transition occurs at a pressure of 28.3 GPa, which is close to the experimentally observed[16] value of 20.5 GPa. Quantitative discrepancies between experimental data and model outputs may be attributed to the model's simplicity and the lack of feedback between solving the impurity problem in DMFT and DFT's lattice degrees of freedom. Our calculations show that
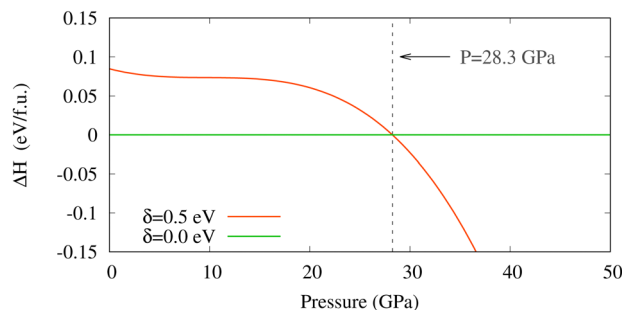
this transition is accompanied by a volume collapse of 1.2%. Although this value is less than the experimental[16] one, the qualitative effect is well reproduced by this oversimplified model. This supports our hypothesis regarding the role of interstitial electronic correlations in the metal-to-semiconductor transition and the volume collapse phenomenon in the Ca_2N during the transformation of the 3D–0D electride subspace.

2.5 Spin-state transition and magnetism

On the next step we used this model, which reliably reproduces the metal-to-semiconductor transition and volume collapse, to analyze changes in magnetic properties during the observed phase transformation. We started with the study of the lifetime of the local moment by analysis of the evaluation of the local spin–spin correlation function $\langle \mathbf{S}_z(\tau)\mathbf{S}_z(0)\rangle$ on the imaginary time axis (Fig. 9) where $\mathbf{S}_z = \sum_{i\sigma\sigma'} \hat{c}^{\dagger}_{i\sigma}\sigma_{\sigma\sigma'}\hat{c}_{i\sigma'}$, $\hat{c}^{\dagger}_{i\sigma}$ and $\hat{c}_{i\sigma'}$ are the electron creation and annihilation operators at orbital i and spin projection σ, $\boldsymbol{\sigma}_{\sigma\sigma'}$ are Pauli matrices.[24–26] Fig. 9 clearly shows the presence of two distinct sets of curves for $\delta \leq 0.2$ eV and $\delta \geq 0.3$ eV, i.e. before and after opening the gap. One can see the qualitative difference in the behavior of the correlation functions between these two sets: in the first case, a very strong dependence on imaginary time is observed, unlike the second case, where the dependence is much less pronounced. This indicates that the lifetime of the local moment in the second phase is significantly longer than in the first phase and that the moments in the second phase are more localized.

We also performed calculations of spin–spin correlation functions for $\delta = 0.0$ and 0.5 eV at various temperatures, from which the local spin susceptibility was derived as $\chi_{\text{loc}} = g_s^2/3 \cdot \int_0^{\beta} d\tau \langle \mathbf{S}(0)\mathbf{S}(\tau)\rangle$, where $g_s = 2$ is the electron spin factor g and $\mathbf{S}$ is the spin operator (inset in Fig. 9). The temperature dependence of χ_{loc} exhibits qualitative differences between the two phases of Ca_2N. In the case of the 3D electride system ($\delta = 0.0$ eV), the behavior indicates the presence of partially localized and relatively large magnetic moments in the interstitial regions. On the other

Fig. 8 Phase diagram with metal-to-semiconductor cross at $P = 28.3$ GPa.
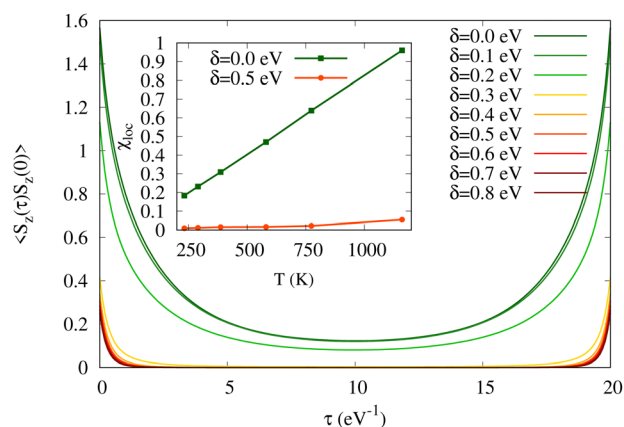
Fig. 9 Local spin–spin correlation functions $\langle S_z(\tau)S_z(0)\rangle$ in the imaginary time domain at $\beta = 20$ eV^{-1} for different values of the crystal field splitting parameter δ. Inset: Temperature dependence of the local spin susceptibility at $\delta = 0.0$ and 0.5 eV.

This journal is © the Owner Societies 2023

Phys. Chem. Chem. Phys., 2023, **25**, 30960–30965 | **30963**
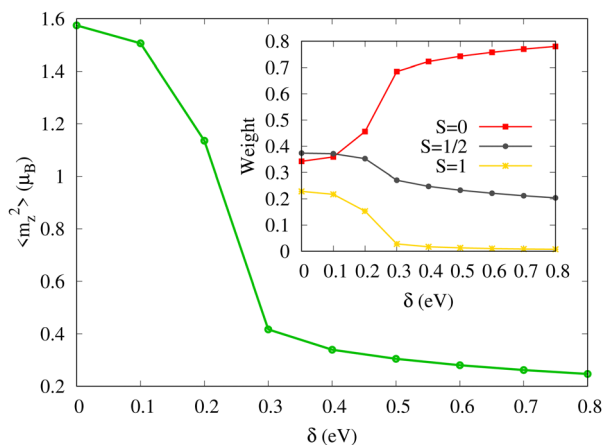
Fig. 10 $\langle m_z^2 \rangle$ and statistical weights in inset.

hand, for the phase corresponding to the 0D electride (δ = 0.5 eV), the local susceptibility is close to zero and practically independent of temperature. Considering that the localization of moments in the 0D phase is significantly higher, one can conclude that the interstitial electrons form a pair with a net magnetic configuration $S = 0$.

The dependence of square of the magnitude of the fluctuating moment $\langle m_z^2 \rangle$ on the crystal field parameter δ shown in Fig. 10 confirms the sharp decrease of local magnetic moment on the interstitial states. The inset in Fig. 10 presents the statistical weights of possible spin states, which clearly show that a spin-state transition occurs during the 3D–0D transition. The statistical weight of the states with spin $S = 1$ decreases almost to zero at $\delta = 0.3$ eV, while the weight of the states with $S = 0$ becomes dominant and approaches 80% as δ increases. This observation supports the model of formation of electron pairs on the interstitial states of Ca_2N during the transition from the $Fd\bar{3}m$ to the $I\bar{4}2d$ phase.

The mechanism described in this paper accompanying the phase transition from 3D to a 0D electride phase under pressure can have universal features that characterize electrides as materials in which Coulomb correlations play an important role in the formation of their observed properties. These include the growth of the degree of localization of interstitial electronic states due to a decrease in the volume of crystal cavities and an increase in the depth of the electrostatic potential well that confined excess electrons. If quasi-atom states are only partially filled, increasing localization leads to a stronger Coulomb interaction between excess electrons. This creates a tendency for a transition from the metallic phase to the insulator or semiconductor phase. Furthermore, a decrease in the symmetry of the crystal environment of the electride cavity promotes and intensifies this transition. This ultimately results in the effect of volume collapse.

3 Conclusion

In summary, we have established that the mechanism of the experimentally observed metal-to-semiconductor transition during the structural transformation from the $Fd\bar{3}m$ to the

$I\bar{4}2d$ phase of Ca_2N under pressure is reminiscent of Mott physics and is driven by correlation effects on interstitial electronic states. Implementation of this mechanism assumes lifting of the symmetry protection of degenerate states in the electride subsystem due to the distortion of the crystal field by the local environment of the electride quasi-atom. Using a simplified model that takes into account the partial reduction of the degeneracy from interstitial electronic states and solving it by DMFT, we were able to reproduce the experimentally observed transition between 3D and 0D electride phases and qualitatively obtain the volume collapse. We have shown that an increase in the strength of correlation effects during the metal-to-semiconductor transition, accompanied by a pronounced enhancement in the localization of electride states and the emergence of pairing of the excess electrons, leads to a spin-state transformation and a drop in the magnetic moment on the interstitial states.

One can expect that the metal-to-semiconductor transition, as well as the spin-state transition between high-spin and low-spin states, is the typical mechanism of the 3D–0D transformation in electrides under pressure and is worth further detailed investigation.

4 Methods

The noninteracting DFT band structure $\varepsilon(\vec{k})$ was obtained using the Quantum ESPRESSO package[27] with the exchange–correlation energy described by the generalized gradient approximation (GGA) and the Perdew–Burke–Ernzerhof (PBE) functional.[28] Structural data for Ca_2N were taken from ref. 16. The MLWF basis was generated using the Wannier90 package,[29] which was also used to extract the noninteracting GGA Hamiltonian H_{GGA} in the real space. The Hamiltonian obtained was converted to reciprocal space using a regular $12 \times 12 \times 12$ k-point mesh, followed by diagonalization. This transformation effectively reduces the off-diagonal elements of the Green's function to negligible values, enabling the utilization of a diagonal solver. DFT+DMFT calculations were performed for the inverse temperature $\beta = 1/k_B T$ from 10 to 50 eV^{-1}, where k_B is the Boltzmann constant and T is the absolute temperature. The effective quantum impurity problem[30] was solved using the continuous-time quantum Monte Carlo method with the hybridization expansion algorithm[31] as implemented in package AMULET.[32]

Author contributions

D. Y. N. conceptualization, investigation and writing – original draft; M. A. M. formal analysis; D. M. K. formal analysis and writing – review & editing; A. O. S. formal analysis and writing – review & editing; V. I. A. writing – review & editing; A. R. O. writing – review & editing, project administration and funding acquisition.

Conflicts of interest

The authors declare no conflicts of interest.

Acknowledgements

References

1 P. P. Edwards, Electrons in Cement, *Science*, 2011, **333**, 49–50.

2 M. S. Miao and R. Hoffmann, High pressure electrides: A predictive chemical and physical theory, *Acc. Chem. Res.*, 2014, **47**, 1311–1317.

3 M.-s Miao and R. Hoffmann, High-Pressure Electrides: The Chemical Nature of Interstitial Quasiatoms, *J. Am. Chem. Soc.*, 2015, **137**, 3631–3637.

4 Q. Zhu, T. Frolov and K. Choudhary, Computational Discovery of Inorganic Electrides from an Automated Screening, *Matter*, 2019, **1**, 1293–1303.

5 D. Y. Novoselov, D. M. Korotin, A. O. Shorikov, A. R. Oganov and V. I. Anisimov, Interplay Between Coulomb Interaction and Hybridization in Ca and Anomalous Pressure Dependence of Resistivity, *JETP Lett.*, 2019, **109**, 387–391.

6 D. Y. Novoselov, D. M. Korotin, A. O. Shorikov, A. R. Oganov and V. I. Anisimov, Weak Coulomb correlations stabilize the electride high-pressure phase of elemental calcium, *J. Phys.: Condens. Matter*, 2020, **32**, 445501.

7 D. Y. Novoselov, D. M. Korotin, A. O. Shorikov, V. I. Anisimov and A. R. Oganov, Interacting Electrons in Two-Dimensional Electride Ca_2N, *J. Phys. Chem. C*, 2021, **125**, 15724–15729.

8 D. Y. Novoselov, V. I. Anisimov and A. R. Oganov, Strong electronic correlations in interstitial magnetic centers of zero-dimensional electride β-Yb_5Sb_3, *Phys. Rev. B*, 2021, **103**, 235126.

9 H. Hosono and M. Kitano, Advances in Materials and Applications of Inorganic Electrides, *Chem. Rev.*, 2021, **121**, 3121–3185.

10 Z. Wan, W. Xu, T. Yang and R. Zhang, As-Li electrides under high pressure: Superconductivity, plastic, and superionic states, *Phys. Rev. B*, 2022, **106**, L060506.

11 S. Liu, C. Wang, H. Jeon, Y. Jia and J.-H. Cho, Emerging two-dimensional magnetism in nonmagnetic electrides Hf_2X (X = S,Se,Te)., *Phys. Rev. B*, 2022, **105**, L220401.

12 Z. Liu, Q. Zhuang, F. Tian, D. Duan, H. Song, Z. Zhang, F. Li, H. Li, D. Li and T. Cui, Proposed Superconducting Electride Li_6C by sp-Hybridized Cage States at Moderate Pressures, *Phys. Rev. Lett.*, 2021, **127**, 157002.

13 A. Fujimori, Electride surface hosts Wigner-crystal melting, *Nat. Mater.*, 2022, **21**, 1217–1218.

14 M. A. Mazannikova, D. M. Korotin, A. O. Shorikov, V. I. Anisimov and D. Y. Novoselov, Electronic Transport via Interstitial States in Mayenite Electride, *J. Phys. Chem. C*, 2023, **127**, 8714–8719.

15 D. Y. Novoselov, M. A. Mazannikova, D. M. Korotin, A. O. Shorikov, M. A. Korotin, V. I. Anisimov and A. R. Oganov, Localization Mechanism of Interstitial Electronic States in Electride Mayenite, *J. Phys. Chem. Lett.*, 2022, **13**, 7155–7160.

16 H. Tang, B. Wan, B. Gao, Y. Muraba, Q. Qin, B. Yan, P. Chen, Q. Hu, D. Zhang and L. Wu, *et al.*, Metal-to-Semiconductor Transition and Electronic Dimensionality Reduction of Ca_2N Electride under Pressure. *Advanced*, *Science*, 2018, **5**, 2–7.

17 Y. Zhang, W. Wu, Y. Wang, S. A. Yang and Y. Ma, Pressure-Stabilized Semiconducting Electrides in Alkaline-Earth-Metal Subnitrides, *J. Am. Chem. Soc.*, 2017, **139**, 13798–13803.

18 Y. Ma, M. Eremets, A. R. Oganov, Y. Xie, I. Trojan, S. Medvedev, A. O. Lyakhov, M. Valle and V. Prakapenka, Transparent dense sodium, *Nature*, 2009, **458**, 182–185.

19 T. Matsuoka and K. Shimizu, Direct observation of a pressure-induced metal-to-semiconductor transition in lithium, *Nature*, 2009, **458**, 186–189.

20 T. Yabuuchi, Y. Nakamoto, K. Shimizu and T. Kikegawa, New High-Pressure Phase of Calcium, *J. Phys. Soc. Jpn.*, 2005, **74**, 2391–2392.

21 N. W. Ashcroft, Pressure for change in metals, *Nature*, 2009, **458**, 158–159.

22 K. Held, I. A. Nekrasov, G. Keller, V. Eyert, N. Blümer, A. K. McMahan, R. T. Scalettar, T. Pruschke, V. I. Anisimov and D. Vollhardt, Realistic investigations of correlated electron systems with LDA + DMFT, *Phys. Status Solidi B*, 2006, **243**, 2599–2631.

23 F. Birch, Finite Elastic Strain of Cubic Crystals, *Phys. Rev.*, 1947, **71**, 809.

24 P. A. Igoshev, A. V. Efremov, A. I. Poteryaev, A. A. Katanin and V. I. Anisimov, Magnetic fluctuations and effective magnetic moments in γ-iron due to electronic structure peculiarities, *Phys. Rev. B: Condens. Matter Mater. Phys.*, 2013, **88**, 155120.

25 A. O. Shorikov, A. I. Poteryaev, V. I. Anisimov and S. V. Streltsov, Hydrogenation-driven formation of local magnetic moments in $LaCoO_3$, *Phys. Rev. B*, 2018, **98**, 165145.

26 D. Y. Novoselov, D. M. Korotin, A. O. Shorikov and V. I. Anisimov, Charge and spin degrees of freedom in strongly correlated systems: Mott states opposite Hund's metals, *J. Phys.: Condens. Matter*, 2020, **32**, 235601.

27 P. Giannozzi, S. Baroni, N. Bonini, M. Calandra, R. Car, C. Cavazzoni, D. Ceresoli, G. L. Chiarotti, M. Cococcioni and I. Dabo, *et al.*, QUANTUM ESPRESSO: a modular and open-source software project for quantum simulations of materials, *J. Phys.: Condens. Matter*, 2009, **21**, 395502.

28 J. P. Perdew, K. Burke and M. Ernzerhof, Generalized Gradient Approximation Made Simple, *Phys. Rev. Lett.*, 1996, **77**, 3865–3868.

29 A. A. Mostofi, J. R. Yates, G. Pizzi, Y.-S. Lee, I. Souza, D. Vanderbilt and N. Marzari, An updated version of wannier90: A tool for obtaining maximally-localised Wannier functions, *Comput. Phys. Commun.*, 2014, **185**, 2309–2310.

30 P. Werner and A. J. Millis, Hybridization expansion impurity solver: General formulation and application to Kondo lattice and two-orbital models, *Phys. Rev. B: Condens. Matter Mater. Phys.*, 2006, **74**, 155107.

31 E. Gull, A. J. Millis, A. I. Lichtenstein, A. N. Rubtsov, M. Troyer and P. Werner, Continuous-time Monte Carlo methods for quantum impurity models, *Rev. Mod. Phys.*, 2011, **83**, 349–404.

32 ''AMULET'', **https://amulet-code.org.**

This journal is © the Owner Societies 2023

Phys. Chem. Chem. Phys., 2023, **25**, 30960–30965 | **30965**